We are IntechOpen, the world's leading publisher of Open Access books
Built by scientists, for scientists

6,900
Open access books available

185,000
International authors and editors

200M
Downloads

154
Countries delivered to

Our authors are among the
TOP 1%
most cited scientists

12.2%
Contributors from top 500 universities

CLARIVATE ANALYTICS
BOOK CITATION INDEX
INDEXED

WEB OF SCIENCE™

Selection of our books indexed in the Book Citation Index
in Web of Science™ Core Collection (BKCI)

Interested in publishing with us?
Contact book.department@intechopen.com

Numbers displayed above are based on latest data collected.
For more information visit www.intechopen.com

Chapter

Effect of Annealing on Metal-Oxide Nanocluster

Naorem Khelchand Singh and Rajshree Rajkumari

Abstract

Recently, the development of optoelectronic devices based on metal-oxide nanocluster has attracted intensive research interest. Nanoclusters are suitable for these because of their large surface-to-volume ratio and the presence of abundant oxygen vacancies or trap states. Metal–oxides such as ZnO, In_2O_3, and TiO_2 synthesized using different technique produces high surface area films consisting of clusters and provides complete control over the film morphology. In this chapter, some of the metal oxides nanocluster film has investigated, and the effect of annealing on the structural, optical and electrical properties of the grown films when subjected to different annealing temperatures will be studied. Theoretically, these properties are presumed to improve after the heat treatment as the crystallinity, and the grain size of the film has increased due to the diminishing of oxygen vacancies. Thus, the greater surface-to-volume ratio, the better stoichiometry and higher level of crystallinity compared to bulk materials make nanocluster-based devices very promising for the mentioned application.

Keywords: nanomaterials, metal oxide semiconductor nanomaterials, fabrication technique, heat treatment, nano-devices

1. Introduction

Surface area and quantum confinement effects are the two important key factors that cause the properties of nanomaterials to differ significantly from the normal bulk materials. Among those nanomaterials, the metal oxide nanoparticles /nanoclusters exhibit unique physical and chemical properties due to their high surface area and nanoscale size. As the particle decreases, a greater amount of atoms are found at the surface compared to those inside. The particle size is influenced to the structural characteristics namely the lattice symmetry and cell parameter) as well as electronic properties in any material. Metal oxide nanocluster finds its promising applications in optical and sensors [1], optoelectronics [2], photocatalysts [3] and biomedical applications [4]. Till now, there have been a considerable number of reports for the fabrication of various metal oxide nanocluster, such as ZnO [5–8], TiO_2 [1, 3, 9], SnO_2 [10–13], In_2O_3 [14–16], CuO_2 [17–19], WO_3 [20, 21]. The reported technique for the synthesis includes (a) physical synthesis such as pulsed laser deposition [5], glancing angle deposition [2], cluster beam deposition [22], and others; (b) chemical synthesis such as sol-gel [9], hydrothermal decomposition [18], and others; (c) biological synthesis using agro wastes, algal media, plant extract, fungi, yeast, and others.

Metal oxide nanocluster in the context of high-performance optoelectronic devices based entirely on the structural, optical and electrical properties. The electrical conductivity of the device strongly depends on the surface defects, grain boundary, surface adsorbed oxygen and unsaturated dangling bonds. In fact, metal oxide nanocluster contains a considerable number of point and surface defects associated with the deviation from the stoichiometric composition. Moreover, the generation of oxygen vacancies in metal oxide nanocluster hampers the efficiency and accuracy of the device. So, in order to reduce the deformation in the surface structure and high defect density related to oxygen vacancies, heat treatment is necessary. Many studies reported on synthesizing metal oxide nanocluster followed by annealing in the different atmosphere. They have shown that annealing at an optimal temperature obtained smooth surfaces, reduced structural defects and improved the crystallinity of the metal oxide nanocluster. Owing to the high surface area of nanocluster, most of the atoms, dangling bonds, and local atomic defects exist at the surfaces texture of nanocluster rather than the inner cores. So, the surface of the nanocluster is unstable and has high chemical activity with a strong tendency to adsorb atoms from the surrounding environments. This active surface area is an essential factor in determining the detection limits or sensitivity. Aluri et al. have demonstrated highly selective and ultra-high sensitive sensors by functionalizing the TiO_2 nanoclusters on the GaN nanowire [23]. The deformation in the surface structure and the local defects acquire a vital role in the optical properties by creating energy bands in the band gap region which is an undesired scope in the field of optoelectronics application. Therefore, we expected that the annealing treatment can trigger the oxygen vacancies and improved the crystal quality of the nanostructure.

In this chapter, we will study the effect of annealing on different metal oxide nanoclusters for different applications. Besides reviewing the literature studied by the various groups, we will be focusing on the report from our research group.

2. Metal oxide nanocluster

2.1 ZnO nanocluster

ZnO is a striking n-type metal-oxide-semiconductor that has a wide bandgap of 3.37 eV, large exciton binding energy of 60 meV and excellent chemical stability, electrical, optical, piezoelectric and pyroelectric properties. ZnO nanostructures have gained tremendous interest due to their potential applications in various nanodevices such as nanogenerators, field emitters, UV detectors, gas sensors, and solar cells. Due to their advanced technological applications, high qualities of zinc oxide nanostructures are greatly demanded.

Xuehua et al. reported the co-doped ZnO nanocluster fabricated by using nanocluster-beam deposition and its effect of annealing at 400 and 700°C on the structural, optical and magnetic properties for diluted magnetic semiconductors (DMSs) [24]. The XRD pattern showed the enhanced crystalline structure by increasing the annealing temperature. A possible explanation is that as grown nanoclusters were highly porous after the random nucleation of atoms under nanocluster-beam deposition. However, after annealing in air, the crystallite sizes were increased from 6 to 20 nm with fewer defects due to the agglomeration of nearby nanoclusters from the obtained thermal kinetic energy. It was also found that the absorption spectra of the annealed film become steeper as compared to the prepared sample. A blue shift appeared at 368 nm (3.37 eV) in the as-grown film mainly due to the quantum confinement effects. However, after annealing at

400°C, a redshift at 365 nm (3.39 eV) observed due to the increased in the crystallite size induced by annealing. But, no change appeared as the annealing temperature increased to 700°C. The intensity has decreased after annealing in the range of 210–350 nm which indicate that the annealed sample attained more enhanced structure and crystallinity. A strong UV emission observed at 379 nm caused by the recombination of surface-bound acceptor-exciton complexes and the peak intensity of the UV emission became stronger after annealing due to the enhanced crystallinity. The film annealed at 400°C exhibited the highest saturation magnetization of 36 μemu. The improvement in saturation magnetization is due to the exchange of F-center mediation [25]. Thus, the results further suggested that the annealing at 400°C strongly affect ferromagnetic performance.

Recently, Aljawfi et al. [26] studied the impact of annealing on the structural and optical properties of ZnO nanoparticles through auto combustion route and annealed in air at different temperatures: 200, 400, 600, and 800°C. They showed that the film annealed at 200°C had a low-quality crystal. As the annealing temperature increased, the crystallite size increased to 37 nm from 13.8 nm. Due to annealing, the crystallites gained enough diffusion or activation energy and small crystallites migrate to relatively equilibrium sites in the crystal lattice with lower surface energy. The room temperature PL spectra with different annealing temperature were also studied. The sample annealed at low temperature (200°C) exhibited anomalous behaviors; where the UV-PL band evidently diminished that indicate the low crystal quality. The results also revealed the presence of clusters in the ZnO NPs associated with low annealing temperature, and the existence of clusters characterized by the diminished and blue shift in the UV band to lower wavelength. The increased in the intensity of UV-PL emission bands and the decreased in the intensity of the VIS-PL band in sequence with further annealing indicated the improvement in the crystallinity and reduction in the intrinsic local atomic defects. They also revealed that the annealing of ZnO clusters at or above 400°C optimized the crystallinity and enhanced the UV spectra related to optoelectronics application.

The heat treatment in air or pure oxygen may promote the reduction in oxygen vacancy and strong emission in ultraviolet band. Gao et al. further confirmed the above statement [27]. They have prepared the ZnO nanocluster porous films on a glass substrate by the successive ionic layer adsorption and reaction (SILAR) method and annealed at 400°C in Argon and air atmosphere for 2 h. A strong diffraction peak of (100) for the sample annealed in the air is obtained which implies that oxygen in the annealing atmosphere can enhance the crystalline properties of ZnO. The film annealed in air/Ar posses increased in the transmittance due to the reduced porosity. Moreover, the peak emission intensity at 380 nm decreased after annealing which indicated the high optical quality of the ZnO layer. The emission at 380 nm corresponds to the intrinsic transition of exciton from the conduction band to the valence band. Thus, they inferred that the annealing in air enhanced the crystalline properties of ZnO rather than annealing in Argon but have no evident effect on the photoluminescence of ZnO film.

We have carried out the fabrication of ZnO nanocluster and SiO_x/ZnO heterostructure nanocluster by using glancing angle deposition (GLAD) technique [28]. Glancing angle deposition (GLAD) technique is a physical vapor deposition technique for producing high-quality nanostructures as shown in **Figure 1**. The advantages of the GLAD technique are as follows: (i) the nanostructure is of high purity as they prepared in an ultra-high vacuum without any catalysts; (ii) the porosity of the nanostructure can be controlled by changing the incident angle; (iii) there is almost no restriction on materials since the growth process is thermal evaporation; (iv) the shape, and in-plane alignment of nanostructure can be easily modified; (v) self-alignment due to the shadowing effect directly on the device substrate
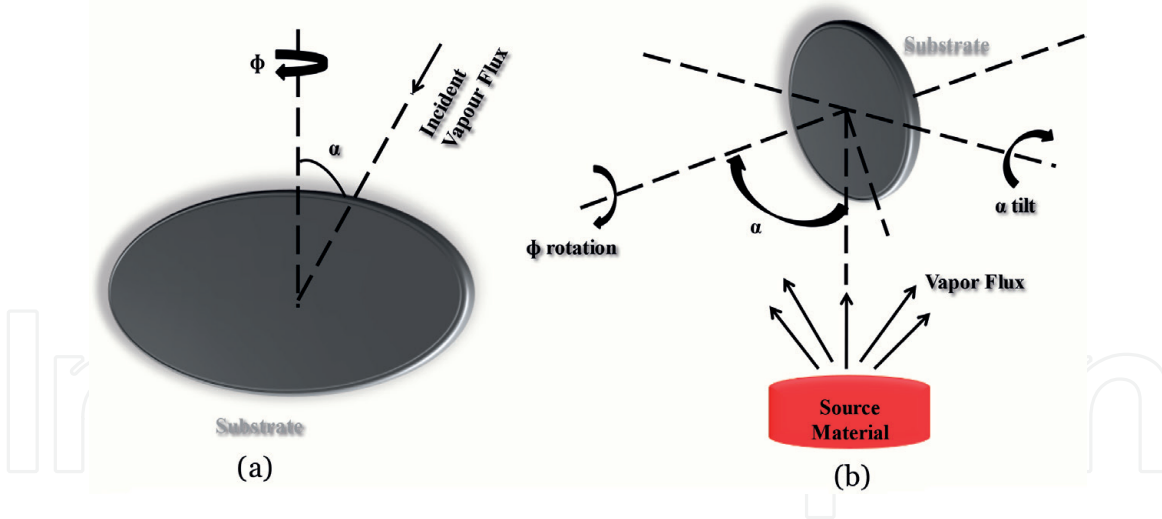
Figure 1.
(a) GLAD about incident angle α of the vapor flux and (b) substrate azimuthally (φ) rotation.

without the need for any additional experimental set up; and (vi) the technique could be used for commercial purposes.

GLAD can be used to engineer the nanostructure films with morphological features such as nanorods, nanowires, nanoclusters, helixes, zigzags, by adjusting the deposition angle, α and substrate rotation angle, φ. In this technique, three parameters determine the morphology of the nanostructure: the incident angle, the growth rate, and the substrate rotational speed. The high melting point materials have relatively low surface mobilities during the film growth processes. Therefore, during the growth process, a high melting point material flux is chosen to be incident onto the surface normal, and the substrate is rotating. GLAD produces nanostructure through the effect of shadowing during film growth with low surface mobilities force the adatoms to form porous nanostructures. Nanostructure films with their high surface to volume ratio are a potential application for optoelectronic devices since their unique morphology can enhance the device performance, namely: photosensitivity, wavelength selectivity, response and reset times, and reproducibility and stability.

The basic deposition setup is the same as that of oblique angle deposition is shown in **Figure 2**; the only difference is that the substrate manipulated by the incident angle Θ and the azimuthal rotation of the substrate concerning the substrate surface normal. By combining the oblique angle deposition and substrate positional control, a technique is introduced which is called glancing angle deposition (GLAD). In this deposition technique, the collimated evaporation beam has a large incident angle α concerning the substrate surface normal therefore incoming vapor can be considered as vector F. This vector F has two components, a vertical component $F_\perp = F \cos \alpha$ and α lateral component $F_\parallel = F \sin \alpha$. The substrate will receive the vapor from both the components, but for the growth of the nanoclusters, the deposition should be preceded by $F_\perp$ only, i.e., cancel out the $F_\parallel$ component. This forms the basis of the glancing angle deposition technique for the growth of nanoclusters. When the substrate rotates azimuthally, each part has an equal chance to receive the same amount of particle from the $F_\parallel$ component. After a complete revolution, the average $\sum F_\parallel$ is zero due to the cancelation of $F_\parallel$ component at the opposite directions which means that there is no preferred orientation of the nanoclusters. By this technique purely nanoclusters will grow at the substrate surface.

The optical properties were carried out on both the samples by a UV–visible NIR spectrophotometer and photoluminescence spectroscopy (HITACHI, F-7000 FL spectrophotometer). Fourier transform infrared radiation methods (PERKIN ELMER, LAMBDA 900) were also carried out on both the samples. The average
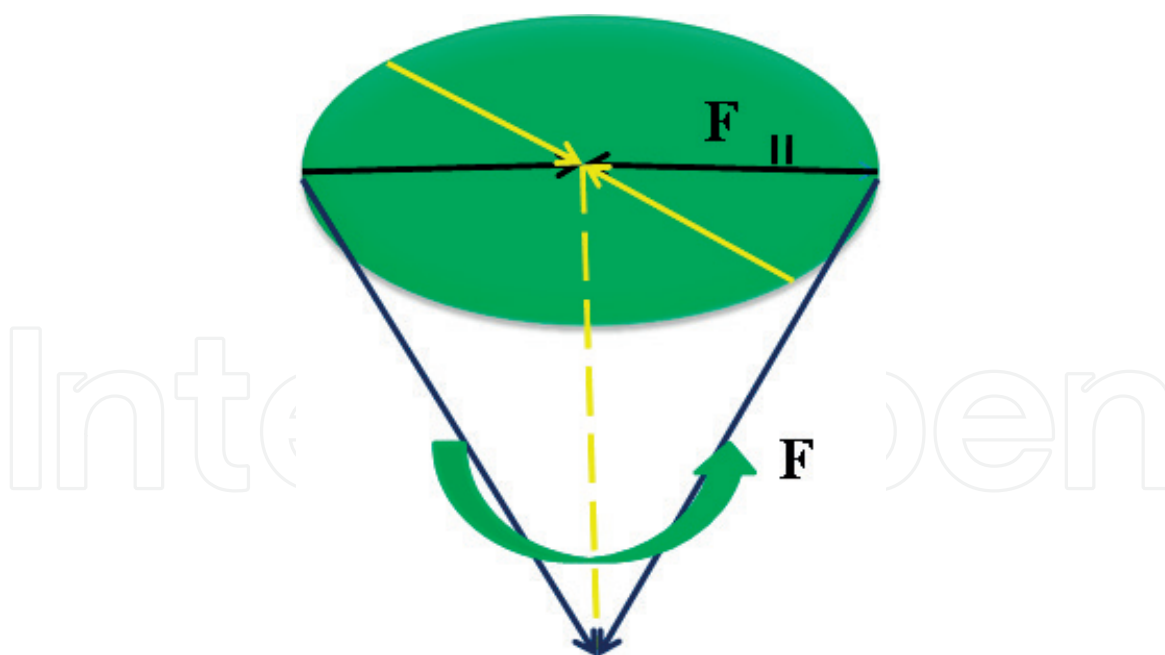
Figure 2.
The cancelation of the $F_∥$ component due to the rotation. Only $F_⊥$ contributes effectively to the increasing height of the nanostructure.

crystallite size of the ZnO nanocluster and SiO$_x$/ZnO heterostructure nanocluster was found to be ~7.101 and ~10.14 nm respectively. The increase in crystallite size suggests the decrease in the existence of grain boundaries in the SiO$_x$/ZnO heterostructure nanocluster [29]. Moreover, the decrease in the average lattice strain observed from 0.01641 (ZnO nanocluster) to 0.01336 (SiO$_x$/ZnO heterostructure nanocluster).

The optical absorption spectrum showed in the wavelength range from 320 to 800 nm of the ZnO nanocluster and SiO$_x$/ZnO heterostructure nanoclusters in **Figure 3**.

ZnO is known to have a large number of defects like oxygen vacancies. When a photon generates an electron-hole pair, recombinations are more likely to take place in the oxygen vacancy. ZnO nanoclusters have a continuous absorption in the UV range as shown in **Figure 3**, demonstrating the presence of a noticeable amount of metallic zinc and a considerable amount of defects [30]. Some recent studies have shown that SiO$_x$ has a conductive property. When electron-hole pairs initially generated in the ZnO nanocluster, the generated electrons accumulate in the conduction band, and they are attracted to the trap level of SiO$_x$ [31]. Hence, due to the presence of SiO$_x$ beneath the ZnO, an enhancement of the light absorption in the visible region beyond 400 nm as well as the near-infrared region can be observed.

The room temperature PL spectra of ZnO nanocluster and SiO$_x$/ZnO heterostructure nanocluster measured under 325 and 350 nm excitation (**Figure 4**). For comparison, PL spectrums showed for both the samples in the same figure. The excitation wavelength of 350 nm exhibits only a strong emission band in the blue region for both the samples attributed to near energy bandgap. The near band gap energy comes from the electron–hole recombination at a deep level (DL) emission in the band gap caused by intrinsic point defects and surface defects, e.g., oxygen vacancies, zinc interstitials. The blue emission peak at 450 nm (~ 2.75 eV) usually results from the radiative recombination of delocalized electrons close to the conduction band with deeply trapped holes in zinc vacancy. The intensity of blue emission under excitation wavelength 325 nm of ZnO nanocluster reduced slightly and exhibited non linear increase-decrease dependence, first increasing, the saturation at the bandgap energy as the optimal excitation energy and finally decreasing
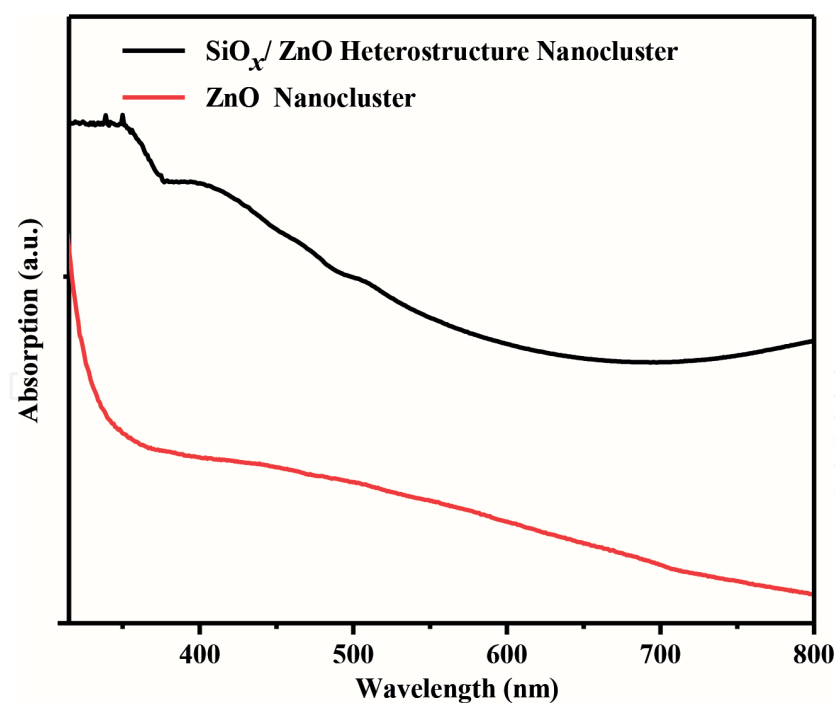
Figure 3.
The optical absorption spectrum of ZnO nanocluster and SiO$_x$/ZnO heterostructure nanocluster.
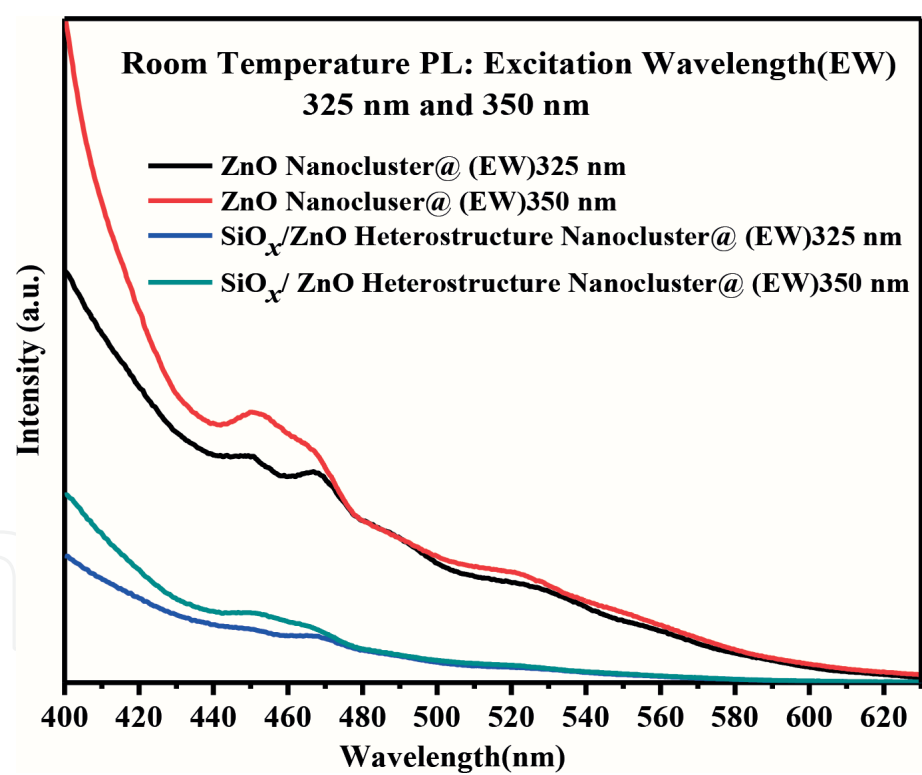

Figure 4.
Photoluminescence spectrum of ZnO nanocluster and SiO$_x$/ZnO heterostructure nanocluster.

but still effectively emitting as slowly dropping tail emission peaks at 467 nm is attributed to the transitions from Zn$_i$ states to the valence band [32].

SiO$_x$/ZnO heterostructure nanocluster exhibited much lower emission intensity than ZnO nanocluster indicating that the recombination of the photogenerated charge carrier significantly inhibited in SiO$_x$/ZnO heterostructure nanocluster. The efficient charge separation may increase the lifetime of the charge carriers and enhance the efficiency of the interfacial transfer to adsorbed substrates and then account for the higher activity. Also, the peak shift from 450 to 457 nm in SiO$_x$/ZnO

heterostructure nanocluster may be due to the radiative recombination of photo-excited electrons. These photoexcited electrons that accumulate in the conduction band of ZnO are attracted to the trap level of SiO_x due to the difference in work functions of ZnO and SiO_x [31].

FTIR spectra of ZnO nanocluster and SiO_x/ZnO heterostructure in the spectral range of 400 to 1500 cm^{-1} shown in **Figure 5** consisted of several bands at 420, 610, 738, 819 and 1109 cm^{-1}. The peak at 420, 610 and 738 cm^{-1} indicates the presence of ZnO which is in good agreement with the results obtained by XRD and attributed to the stretching vibration mode and also be related to the influence of shell induced strain and the appearance of ZnO bond between Zn and O atoms of the shell [33]. The spectra also show the bending vibration of Si—O—Si at 819 cm^{-1} indicating the bonding between the substrate and SiO_x. The peak located at 1109 cm^{-1} assigned to asymmetric Si—O stretching is due to interstitial oxygen impurities dissolved in the Si substrate. In SiO_x/ZnO heterostructure nanocluster, the entire peak transmittance % got quenched. Together these results identified the presence of SiO_x which exist near the ZnO surface.

The above work indicated that the SiO_x/ZnO heterostructure nanocluster could account for higher activity in optoelectronic devices. So, we further annealed the SiO_x/ZnO heterostructure nanocluster at 550°C for 1 h in open air [2]. The annealing treatment was carried out in the muffle furnace. The crystallinity improved after annealing owing to the decrease in the defect density. Also, the increased crystallite size attributed to the coalescence of grains. Moreover, the annealed sample becomes smoother as shown in **Figure 6** and offer a large surface area ascribed to the agglomeration of smaller nanocluster. The authors also confirmed that the oxygen content increased to 20.90% due to the adsorption of O_2 at the time of open-air annealing and hence, absorption is enhanced in the case of the annealed sample as shown in inset **Figure 6**.

The authors also reported the optical absorption spectrum in **Figure 7(a)** of the wavelength range from 320 to 900 nm of the bare ZnO nanocluster, as deposited and annealed SiO_x-ZnO heterostructure nanoclusters. An enhancement of averagely 1.5 times photon absorption is observed in the annealed sample with sharper band edge which indicated the formation of the improved crystal structure of the sample [30]. However, the decreased in the absorbance after annealing in the
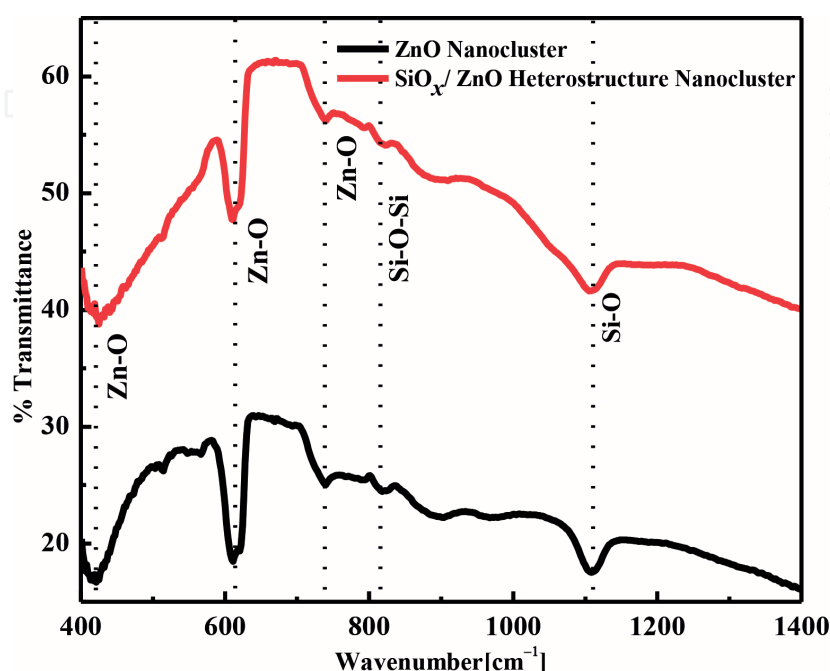

Figure 5.
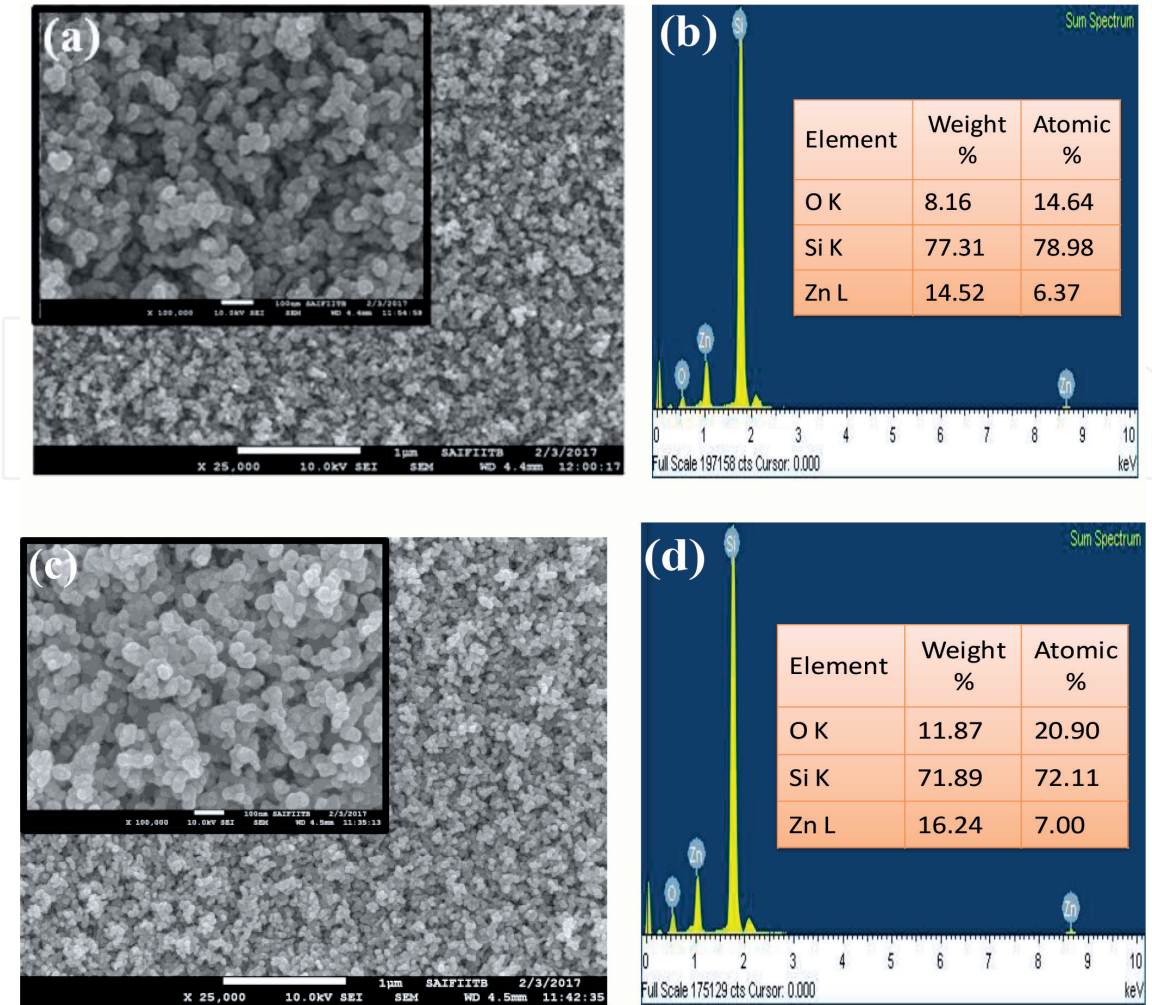*FTIR spectra of ZnO nanocluster and SiO_x/ZnO heterostructure nanocluster.*

Figure 6.
FEG-SEM images of the SiOₓ-ZnO heterostructure nanoclusters: (a) top view (as deposited); (b) EDAX analysis of as-deposited; (c) annealed and (d) top view (annealed).

wavelength range of ~374 to 478 nm is attributed to the change in the band gap. A continuous absorption is seen in the visible range of the as a deposited sample due to the noticeable amount of metallic zinc and a considerable amount of defects. The light absorption is enhanced in the visible region beyond 400 nm to NIR regions. Additionally, the voids were filled up with the O_2 after annealing which enhanced the probability of main band transitions and therefore the absorption in the UV region. Also, the subband transition of SiO_x shows the maximum absorption of at around 2.7 eV in the visible region. The interaction between Si-Si increased and formed the Si nanocluster in the SiO_x due to annealing. The absorption is in the near infrared region is due to the presence of Si. However, no light absorption beyond 850 nm was observed because Si absorbed light efficiently up to near infrared region only. That is why there is a steep change of absorption at 850 nm.

We have obtained the increase in the transmittance after annealing which attributed to the decreased in defects and an increase in the ZnO to Zn ratio [30]. The absorbed oxygen after annealing fills up the oxygen vacancies, hence reducing the density of this donor like defects. The main band gap of ZnO film is 3.37 eV [34]. However, the band gap of the as deposited SiO_x-ZnO heterostructure nanocluster is found to be 2.94 eV due to the downward shift of the conduction band. The less band gap associated with many-body interactions between the carriers in the conduction band and valence band called bandgap renormalization [35]. However, after annealing, the optical band gap increases to 3.44 eV which is influenced by the change in charge carriers and can be explained by Burstein Moss (BM) effect [35].
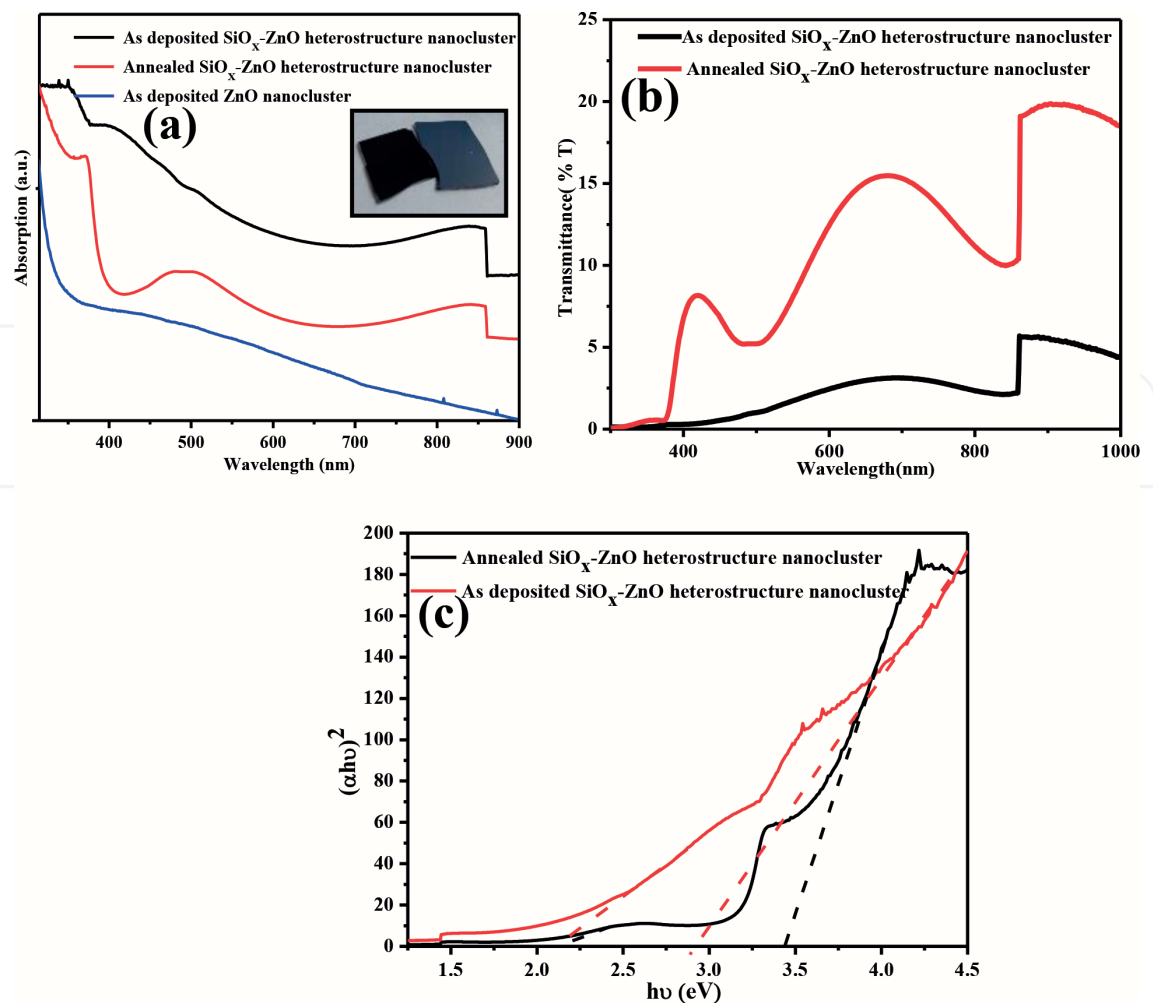
Figure 7.
(a) Optical absorption of as deposited ZnO nanocluster, as deposited and annealed SiO$_x$-ZnO heterostructure nanocluster and (b) transmittance (c) (αhυ)^2 versus hυ curve of as deposited and annealed SiO$_x$-ZnO heterostructure nanocluster.

The PL spectra of the as deposited and annealed SiO$_x$-ZnO heterostructure nanoclusters with different excitation wavelengths of 325, 350 and 375 nm under same 370 filter (**Figure 8**) also studied. The peak intensity significantly increased due to the formation of O$_i$ and O$_{Zn}$ after annealing at 550°C. Generally, the emission peak of ZnO nanostructure centered at around 415 nm. This emission peak arises due to the radiative defects in ZnO. However, in our case, the emission peak at around 420 nm is due to the radiative recombination of photoexcited electrons. These photoexcited electrons that accumulate in the CB of ZnO are attracted to the trap level of SiO$_x$ due to the difference in work functions of ZnO and SiO$_x$. The intensity of blue emission exhibited a non linear increase-decrease dependence, first increasing, the saturation at the bandgap energy as the optimal excitation energy and finally decreasing but still effectively emitting as slowly dropping tail emission peaks at 450 nm and 468 nm which attributed to the transitions from Zn$_i$ and extended Zn$_i$ states to the valence band respectively. These extended states formed during the annealing process according to the defect ionization reaction [32].

2.2 TiO$_2$ nanocluster

Titanium dioxide (TiO$_2$) is a wide bandgap semiconductor with an indirect optical bandgap ranging from 3.2 eV for the anatase phase to 3.0 eV for the rutile phase. The unique physical, chemical, and optical properties have motivated more researchers in many applications such as sensors, photo-electrochemical water
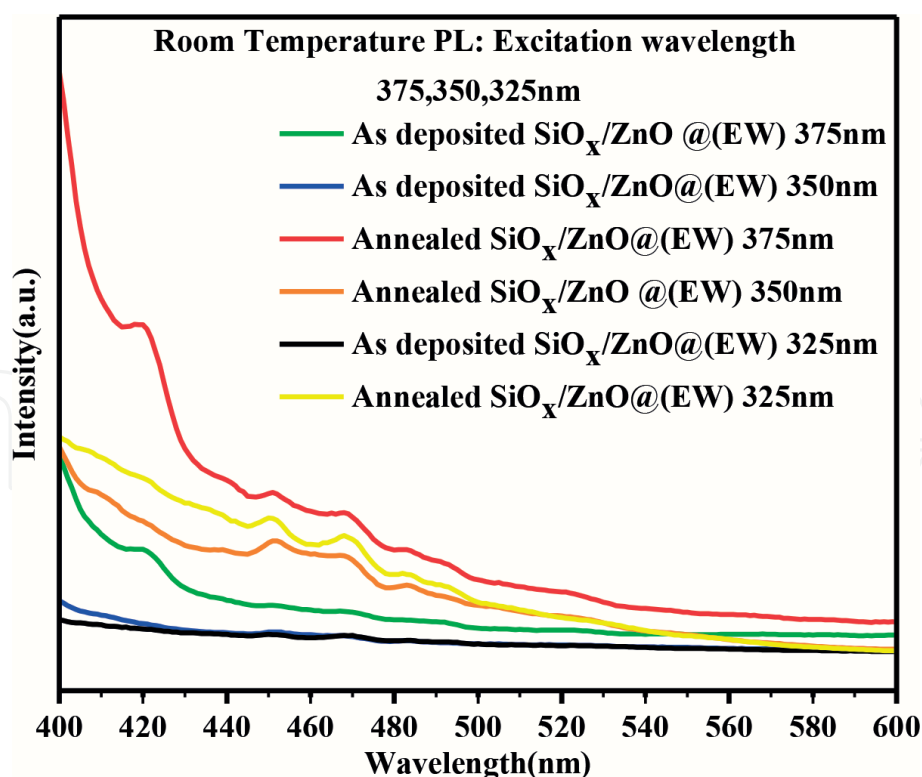
Figure 8.
Photoluminescence spectrum of as deposited and annealed SiO_x-ZnO heterostructure nanocluster.

splitting, dye-sensitized solar cells, photo-catalytic performance, memory devices, and photodetector.

The surface area of the nanostructure is one of the essential factors in determining the sensitivity of the chemical sensors. However, the surface/adsorbate interactions of the nanowires are often limited and non-specific. So, the functionalization of the NWs surface with metal/metal oxide nanoparticle or nanocluster focus at resolving the deficiencies of the NW-based devices. GS Aluri et al. demonstrated GaN nanowires decorated with TiO_2 nanoclusters for selectively sensing benzene and related aromatic environmental pollutants such as toluene, ethylbenzene and xylene [23]. The TiO_2 nanoclusters act as catalysts design to increase the sensitivity, lower the detection time since nanoclusters/nanoparticles can increase the adsorption of chemical species by introducing additional adsorption sites. Herein, TiO_2 nanoclusters fabricated by using RF magnetron sputtering followed by an annealing at 650–700°C in a rapid thermal processing system of ultrahigh purity Ar. The TiO_2 were amorphous in as-deposited film. Upon annealing of TiO_2 nanoclusters at 700°C for 3 s, the phase changed to anatase in the TiO_2 clusters. The I-V curve was nonlinear and asymmetric in the as a deposited sample but the current increased with the deposition of TiO_2 nanoclusters and significant change occurred when the device annealed at 700°C. They have also shown that the photoconductivity increased almost two orders of magnitude for the device decorated with TiO_2 nanoclusters. The enhancement of photoconductance after decorating nanoclusters to nanowires is attributed to the separation of photogenerated charge carriers by a surface depletion field, thereby increasing the lifetime of the photogenerated carriers. Thus, these results demonstrated the potential of hybrid chemical sensors using TiO_2 nanoclusters.

Wei et al. have prepared the *R*-TiO_2 clusters by post-deposition oxidation of Ti clusters with rapid thermal annealing in an oxygen atmosphere [36]. The *R*-TiO_2 clusters showed the highest crystalline structure as compared to Ti, TiO, and A-TiO_2. In a different work, Ag-TiO_2 nanocomposite was prepared by DC reactive magnetron sputtering followed by vacuum annealing treatment from 200 to 800°C.

The friction coefficient increased from 0.21 to 0.7 after the sample annealed at 800°C [37]. Recently, Song et al. fabricated the TiO_2 nanocluster-SiO_x (x˅2) using atomic layer deposition (ALD) for the properties of resistive switching. They performed thermal annealing in N_2 ambient at 900°C for 3 h using a thermal furnace. They have reported the current on/off ratio of the device is about 10^5 (reading at +1.0 V), which is much higher than that of many Resistance change random access memories (RRAM) devices of TiO_2 [38].

TiO_2 nanocluster determined the photocatalytic activity by its crystalline phase (anatase and rutile), crystallite size, specific surface area, pore structure, and crystallinity. Khan et al. reported that the crystallization of TiO_2 film to anatase crystal phase starts occurring at the annealing temperature of 300–600°C in the air which improves the crystal structure of the TiO_2 anatase [39]. Bin et al. investigated the effect of GLAD on TiO_2 nanostructure with different annealing temperature for the morphology, and crystallization and PL. The average size increased with the increase in annealing temperature, and defects were reduced [40].

Min Liu et al. reported the photochemically inactive Ti3+ self-doped TiO_2 prepared by a facile one-step thermal oxidation into an efficient visible light-sensitive photocatalyst by the grafting of Cu (II) oxide amorphous nanoclusters [41]. The grafting of Cu (II) oxide onto TiO_2@Ti3+ performed by the impregnation method shown that the grafting of Cu (II) nanoclusters to TiO_2 increased the absorption intensities in the 420–550 and 700–800 nm wavelength regions assigned to the interfacial charge transfer (IFCT) VB electrons to surface-grafted Cu (II) nanoclusters. On the contrary, the grafting of Cu (II)-TiO_2@Ti3+ the absorption intensities decreased slightly in the range of 420–550 nm wavelength region, while the increased in the absorption intensities can also be observed in the range of 700–800 nm wavelength region attributed to the d-d transition of Cu(II). They have shown that the TiO_2@ Ti3+ had a negligible activity either under visible light or UV light irradiation without the grafting of nanocluster. After grafting, they have switched to an efficient photocatalyst. Further, they have studied the photocatalytic activities of Cu (II)-TiO_2@Ti3+ under visible light irradiation at 400–530 nm (1 mW/cm^2) with different annealing temperature. However, the ratio of TiO_2 to Ti_2O_3 greatly influenced the morphology and the degree of oxidation states rather than annealing.

2.3 Tungsten oxide nanocluster

In the family of metal transition oxides, tungsten trioxide (WO_3) have attracted due to their distinctive properties such as chromogenic properties, gas sensitivity, and photosensitivity. Tungsten oxide nanoclusters were fabricated using supersonic cluster beam deposition (SCBD) by Zhao et al. [21] for examining the H_2 sensing properties. Further, the sample was post-annealed at 250°C for 12 h. They showed a large sensor signal of 1200 at 3000 ppm of H_2 in the air due to the small cluster size. The response of H_2 was over a broad range from 4 to 20,000 ppm. Moreover, the detection limit is as low as 0.042 ppm. Lastly, the sensor exhibit fast response rate.

2.4 Iron oxide nanocluster

The unique properties such as superparamagnetism arise from the fluctuation in the direction of the magnetic moment in a single domain nanoparticle due to thermal agitation. Marin et al. reported a novel core-shell superparamagnetic iron oxide nanocluster under annealing treatment [42]. The annealing of iron oxide nanocluster at 300°C for 3 h in air greatly influences the magnetic properties. Due to the thermal decomposition of the surfactants during the annealing treatment and in the absence of oxygen inside the nanoclusters led to the formation of an amorphous

carbon" coat" around the maghemite nanoparticle. After the annealing treatment, the value of saturation magnetization is increased by about ~13.6%. This increase in the magnetization of the annealed sample can be attributed to the degradation and decomposition of the surfactants and their release of gas products during the annealing treatment from the sample, i.e. to the higher content of the magnetic material in the annealed sample. They showed the decrease in the interactions in the annealed sample indicated that the maghemite nanoparticles are better isolated and shield each other with the amorphous carbon.

Apart from the nanoclusters, the effect of annealing on metal oxide nanostructures such as indium oxide and tin oxide will be discussed in the next section.

2.4.1 Indium oxide

Indium oxide (In_2O_3), known as an n-type, is a wide-bandgap transparent semiconductor (with a direct bandgap of ~3.6 eV and an indirect bandgap of ~2.5 eV) is of great interest for diverse technological applications in nanoelectronics and optoelectronics. Zero-dimensional In_2O_3 nanoparticles/nanoclusters, with a variety of tunable, are beneficial as building blocks for indium oxide-based or hybrid transistor. Their remarkably surface-to-volume ratio and good stability have made them promising materials in gas sensors/biosensors, photocatalysis, photoelectrochemical cells, and ultraviolet photodetectors. Despite the advantages, In_2O_3 nanostructure usually encounters low conductivity, and this could decrease the stability and efficiency of the device. Due to the weak interconnection between the nanoparticles/nanoclusters, the carrier transportation between the NPs lost at the interface due to the charge delocalization. One way to solve this problem is to improve the structure by annealing and plasma treatment.

Kong et al. reported the zero-dimensional In_2O_3 nanoparticle sample showed an improvement in the crystallinity and a more compact structure after the thermal treatment [43]. It also showed an improvement in the optical and electrical properties of the In_2O_3 nanoparticle. Flores et al. studied the effect of annealing on the electrical, optical and structural properties of the undoped In_2O_3 nanostructure [44]. The film first annealed at 300°C in the air and the second annealing at 500°C results with a better passivation effect of the traps, whether located at grain boundaries or in the bulk of the indium oxide grains. So, the highest carrier concentration, mobilities, and band gap value obtained for the samples treated under 300 and 500°C. Sudha et al. [45] also investigated the crystallinity of In_2O_3 nanostructures along with the grain size augmented with annealing temperature. They observed that average grain size increased with increasing annealing temperature and explained by considering the thermal annealing-induced coalescence of small grains by grain boundary diffusion which caused significant grain growth. Microstrain and dislocation density present in the In_2O_3 nanostructure are found to decrease due to thermal annealing implies that the stress is compressive which is likely to be governed by the dominant crystallization process. Senthilkumar et al. presented the influence of annealing temperature on the structural and optical properties of the In_2O_3 films deposited by electron beam evaporation technique in the presence of oxygen [46]. They have also proved that the crystallinity of In_2O_3 films improved with annealing temperature. The optical band gap is found to vary from 3.65 to 3.86 eV with increasing annealing temperature. The shift in the band gap to higher energies attributed to the increase in carrier density which arises from the filling of states near the bottom of the lowest state in the conduction band. The results also show that by increasing the annealing temperature, the electrical resistivity of In_2O_3 thin films decreases which is related to the increase of the mobility and carrier density. Thus, the annealing temperature plays a vital role in the conductivity of the In_2O_3 nanostructure as well.

2.4.2 Tin oxide

In recent years SnO_2 has attracted a lot of interest because of its outstanding electrical, optical and electrochemical properties and these properties enabled the application of SnO_2 in solar cells, catalytic support materials, transparent electrodes, and solid-state chemical sensors. Among the various phases of tin oxides, SnO is the most metastable phase, which is mostly formed at high annealing temperatures (450 and 750°C). The size, morphology, and phase of the tin oxide nanoparticles can be effectively modified by the process of annealing. The effect of pH and annealing temperature on the properties of tin oxide nanoparticles prepared by the sol–gel method has reported [47]. The samples were annealed at 200, 400, 600, and 800°C. The average crystallite size increased with the increase in annealing temperature. The surface morphology of the tetragonal SnO_2 nanoparticles studied by scanning electron microscope revealed the formation of spherically shaped agglomerations.

On the other hand, carbon nanomaterials composed of sp^2 bonded graphitic carbon are found in different dimensions including zero-dimensional fullerenes, one-dimensional carbon nanotubes (CNTs), and two-dimensional graphene. Owing to the unique structure and physical properties, carbon-based nanomaterials have gained lots of interests in electronic, optoelectronic, photovoltaic, and sensing applications. Among the different carbon nanomaterials, CNTs provides unique opportunities for novel optoelectronic properties since semiconducting CNTs are direct bandgap materials that possess free electron-hole pair excitations as well as strongly bound electron-hole pair states called excitons. One dimensional nature of CNTs produces van Hove singularities in the density of states that result in strong optical absorption and emission with energies. The use of graphene for optoelectronic devices is limited due to its zero band gap at the Fermi level. However, by tuning the band gap, graphene can be an ideal candidate for optoelectronic devices [48]. CNTs are also chemically inactive due to their strong sp^2 bonding in a near perfect hexagonal network and this prevents the formation of chemical bonds with most molecules. Its reactivity can be improved towards different gases by decorating the CNTs wall by metal or metal oxide nanocluster due to its physico-chemical properties (e.g. high catalytic activity, adsorption capacity, efficient charge transfer, etc.). Nanoclusters play a major role in the gas detection pathway, in which sensitivity and selectivity can be tuned based on the reactivity of the nanoclusters surfaces and on the nature of the charge transfer between carbon nanotubes and nanoclusters induced by gas adsorption [12]. In addition, the incorporation of metal nanoclusters (Ag, Au) inside carbon host matrix can add functionality to carbon films. However, the high internal stress of carbon can affect the structural evolution of metal incorporated carbon film. Jose et al. [49] studied the influence of annealing in argon at 300°C on the conductivity, phase stability and electronic structure of hydrogen-free amorphous carbon (a-C) films containing copper (aC:Cu) and gold (a-C:Au) nanoclusters. They showed that the a-C host matrix increased its graphitic character and stress was relieved upon annealing due to increase in the high energy side of the σ^* region. Also, the structural transformation after annealing the carbon incorporated nanoclusters changes their electronic conductivity and apparent optical bandgap.

3. Conclusions

The chapter reviewed the effect of annealing on ZnO, SiO_x, and TiO_2 nanocluster for different applications. ZnO, SiO_x, and TiO_2 have been fabricated using

different physical and chemical method. Our work demonstrated the influence of annealing on optoelectronics properties on GLAD synthesized SiO_x-ZnO heterostructure nanoclusters. The post-annealing treatment in oxygen ambient improved the structural, optical and electrical properties. Nanocluster based devices outperform their bulk counterparts. In addition, some different metal oxide nanostructure and its effect of annealing also discussed. Therefore, we may conclude that future nanodevices based on nanocluster should be paid attention to the industrial and commercial applications.

Acknowledgements

The authors would like to thank especially the initiator of this book for making them a part of this vital endeavor.

Conflict of interest

The author declares that there is no conflict of interests regarding the publication of this book chapter.

Appendices and nomenclature

V_{Zn}	zinc vacancy
O_i	oxygen interstitial
O_{Zn}	antisite oxygen
Zn_i	interstitial zinc ion

Author details

Naorem Khelchand Singh[*] and Rajshree Rajkumari
Department of Electronics and Communication Engineering, National Institute of Technology, Nagaland, Dimapur, India

*Address all correspondence to: khelchand.singh@gmail.com

IntechOpen

References

[1] Liu H, Yang W, Wang M, Xiao L, Liu S. Fabrication of lotus-like Au@ TiO₂ nanocomposites with enhanced gas sensing properties. Sensors and Actuators B. 2016:236-490. DOI: 10.1016/j.snb.2016.06.039

[2] Rajkumari R, Singh NK. Influence of annealing on the optoelectronic properties of the GLAD synthesized SiO$_x$–ZnO heterostructure nanoclusters. Applied Physics A: Materials Science & Processing. 2018:124-264. DOI: 10.1007/s00339-018-1687-1

[3] Frederick RT, Novotny Z, Netzer FP, Herman GS, Dohnalek Z. Growth and stability of titanium dioxide nanoclusters on graphene/Ru (0001). The Journal of Physical Chemistry. B. 2018:122-640. DOI: 10.1021/acs.jpcb.7b05518

[4] Lu Y, Xu YJ, Zhang GB, Ling D, Wang MQ, Zhou Y, et al. Iron oxide nanoclusters for T 1 magnetic resonance imaging of non-human primates. Nature Biomedical Engineering. 2017;**1**(8): 637-643. DOI: 10.1038/s41551-017-0116-7

[5] Dinh LN, Schildbach MA, Balloch M, McLean IIW. Pulsed laser deposition of ZnO nanocluster films by Cu-vapor laser. Journal of Applied Physics. 1999:86-1149. DOI: 10.1063/1.370857

[6] Slaughter G, Sunday J. Fabrication of enzymatic glucose hydrogel biosensor based on hydrothermally grown ZnO nanoclusters. IEEE Sensors Journal. 2014:14-1573. DOI: 10.1109/JSEN.2014.2298359

[7] Li X, Zhao Z. Co-doped ZnO thin films fabricated by a nanocluster-beam deposition system and the influence of flow rate of helium gas on their properties. Journal of Superconductivity and Novel Magnetism. 2016;**29**:357. DOI: 10.1007/s10948-015-3230-3

[8] Wu S, Yuan N, Xu H, Wang X, Schelly ZA. Synthesis and bandgap oscillation of uncapped, ZnO clusters by electroporation of vesicles. Nanotechnology. 2006:17-4713. DOI: 10.1088/0957-4484/17/18/031

[9] Liu M, Inde R, Nishikawa M, Qiu X, Atarashi D, Sakai E, et al. Enhanced photo activity with nanocluster-grafted titanium dioxide photocatalysts. ACS Nano. 2014:8-7229. DOI: 10.1021//nn5 10.1021/nn502247x

[10] Yeow SC, Ong WL, Wong ASW, Ho GW. Template-free synthesis and gas sensing properties of well-controlled porous tin oxide nanospheres. Sensors and Actuators B: Chemical. 2009: 143-295. DOI: 10.1016/j.snb.2009.08.050

[11] Lassesson A, Schulze M, Lith JV, Brown SA. Tin oxide nanocluster hydrogen and ammonia sensors. Nanotechnology. 2008:19-015502. DOI: 10.1088/0957-4484/19/01/015502

[12] Leghrib R, Pavelko RG, Felten A, Vasiliev A, Cané C, Gràcia I, et al. Gas sensors based on multiwall carbon nanotubes decorated with tin oxide nanoclusters. Sensors and Actuators B: Chemical. 2010:145-411. DOI: 10.1016/j.snb.2009.12.044

[13] Salavati-Niasari M, Mir N, Davar F. A novel precursor for the synthesis of metallic copper nanocrystals by thermal decomposition approach. Applied Surface Science. 2010:256-4003. DOI: 10.1016/j.apsusc.2010.01.067

[14] Amoli V, Farooqui S, Rai A, Santra C, Rahman S, Sinha A, et al. Indium oxide nanocluster doped TiO₂ catalyst for activation of molecular O₂. RSC Advances. 2015;**5**. DOI: 10.1039/C5RA13104A

[15] Amoli V, Malayil MGS, Banerjee B, Anand M, Maurya A, Farooqui S, et al.

Faceted titania nanocrystals doped with indium oxide nanoclusters as a superior candidate for sacrificial hydrogen evolution without any noble-metal Co catalyst under solar irradiation. ACS Applied Materials & Interfaces. 2014;**7**. DOI: 10.1021/am507293b

[16] Walsh A, Woodley S. Evolutionary structure prediction and electronic properties of indium oxide nanoclusters. Physical Chemistry Chemical Physics. 2010:12-8446. DOI: 10.1039/c0cp00056f

[17] Ayesh A I, Abu Hani A, Mahmoud S, Haik Y. Selective H_2S sensor based on CuO nanoparticles embedded in organic membranes. Sensors and Actuators B: Chemical. 2016:231. DOI: 10.1016/j.snb.2016.03.078

[18] Yin G, Nishikawa M, Nosaka Y, Nagarajan S, Atarashi D, Sakai E, et al. Photocatalytic carbon dioxide reduction by copper oxide nanocluster-grafted niobate nanosheets. ACS Nano. 2015: 9-2111. DOI: 10.1021/nn507429e

[19] Lomnicki S, Wu H, Osborne NS, Pruett J, M, McCarley RL, Poliakoff E, et al. Size-selective synthesis of immobilized copper oxide nanoclusters on silica. Materials Science and Engineering: B. 2010:175-136. DOI: 10.1016/j.mseb.2010.07.016

[20] Tiwari A, Nagaiah TC, Bordoloi A. Electrocatalytic activity of tungsten oxide nanoclusters grafted on mesoporous nitrogen-rich carbon material in the dioxygen reduction reaction. ChemPlusChem. 2015;**80**. DOI: 10.1002/cplu.201500253

[21] Zhao M, Xing Huang J, Wo Ong C. Room-temperature resistive H_2 sensing response of Pd/WO_3 nanocluster-based highly porous film. Nanotechnology. 2012:23-315503. DOI: 10.1088/0957-4484/23/31/315503

[22] Wegner K, Piseri P, Tafreshi H, Milani P. Cluster beam deposition:

A tool for nanoscale science and technology. Journal of Physics D: Applied Physics. 2006;**39**:439. DOI: 10.1088/0022-3727/39/22/R02

[23] Aluri GS, Motayed A, Davydov AV, Oleshko VP, Bertness KA, Sanford KA, et al. Highly selective GaN-nanowire/TiO_2-nanocluster hybrid sensors for detection of benzene and related environment pollutants. Nanotechnology. 2011:22-295503. DOI: 10.1088/0957-4484/22/29/295503

[24] Li X, Zhao Z. Effect of annealing on Co-doped ZnO thin films prepared by nanocluster-beam deposition. Journal of Superconductivity and Novel Magnetism. 2016;**29**:1897. DOI: 10.1007/s10948-016-3395-4

[25] Zhao ZW, Tay BK, Chen JS, Hu J, Sun X, Tan ST. Optical properties of nanocluster-assembled ZnO thin films by nanocluster-beam deposition. Applied Physics Letters. 2005:87. DOI: 10.1063/1.2149170

[26] Aljawfi R, Alam M, Rahman F, Ahmad S, Shahee A, Kumar S. Impact of annealing on the structural and optical properties of ZnO nanoparticles and tracing the formation of clusters via DFT calculation. Arabian Journal of Chemistry. 2018. DOI: 10.1016/j.arabjc.2018.04.006

[27] Gao X. Synthesis and optical properties of ZnO nanocluster porous films deposited by a modified SILAR method. Applied Surface Science. 2004;**229**:275-281. DOI: 10.1016/S0169-4332(04)00104-7

[28] Robbie K, Brett M. Method of depositing shadow sculpted thin films. US Patent 5. 1999:866-204

[29] Akgul G, Akgul FA, Unalan HE, Turan R. Photovoltaic performance of gallium-doped ZnO thin film/Si nanowires heterojunction diodes. Philosophical Magazine. 2016:96-1093. DOI: 10.1080/14786435.2016.1154207

[30] Agarwala DC, Chauhan RS, Kumar A, Kabiraj D, Singh F, Khan SA, et al. Synthesis and characterization of ZnO thin film grown by electron beam evaporation. Journal of Applied Physics. 2006:99-123105. DOI: 10.1063/1.2204333

[31] Dhar JC, Mondal A, Singh NK, Chakrabartty S, Bhattacharyya A, Chattopadhyay KK. Effect of annealing on SiO_x-TiO_2 axial heterostructure nanowires and improved photodetection. Journal of Applied Physics. 2013:114-244310. DOI: 10.1063/1.4858420

[32] Zeng H, Duan G, Li Y, Yang S, Xu X, Cai W. Blue luminescence of ZnO nanoparticles based on non-equilibrium processes: Defect origins and emission controls. Advanced Functional Materials. 2010:20-561. DOI: 10.1002/adfm.200901884

[33] Raevskaya AE, Panasiuk YV, Stroyuk OL, Kuchmiy SY, Dzhagan VM, Milekhin AG, et al. Spectral and luminescent properties of ZnO–SiO_2 core-shell nanoparticles with size-selected ZnO cores. RSC Advances. 2014;**4**:63393. DOI: 10.1039/c4ra07959k

[34] Rodnyi A, Khodyuk IP. Optical and luminescence properties of zinc oxide. Optics and Spectroscopy. 2012;**111**. DOI: 10.1134/S0030400X11120216

[35] Jeon JW, Jeon DW, Sahoo T, Kim M, Baek JH, Hoffman JL, et al. Effect of annealing temperature on optical band-gap of amorphous indium zinc oxide film. Journal of Alloys and Compounds. 2011:509-10062. DOI: 10.1016/j.jallcom.2011.08.033

[36] Wei X, Skomski R, Balasubramanian B, Sun ZJ, Sellmyer D. Magnetism of TiO and TiO_2 clusters. Journal of Applied Physics. 2009: 105-07C517. DOI: 10.1063/1.3074509

[37] Munteanu D, Torrell M, Cunha L, Alves E, Barradas N, Cavaleiro A, et al. The influence of annealing treatments on the properties of Ag:TiO_2 nanocomposite films prepared by magnetron sputtering. Applied Surface Science. 2012:258-4028. DOI: 10.1016/j.apsusc.2011.12.095

[38] Song S, Kim K, Ho Jung K, Sok J, Park K. Properties of resistive switching in TiO_2 nanocluster-SiO_x (X<2) matrix structure. Journal of Semiconductor Technology and Science. 2018:18-108. DOI: 10.5573/JSTS.2018.18.1.108

[39] Khan Abdul F, Mehmood M, Durrani S, L, Ali M, Abd Rahim N. Structural and optoelectronic properties of nanostructured TiO_2 thin films with annealing. Materials Science in Semiconductor Processing. 2014:29. DOI: 10.1016/j. mssp.2014.02.009i

[40] Wang B, Qi H, Chai Y, Li M, Guo M, Pan M, et al. Alteration of titanium dioxide material properties by glancing angle deposition plus annealing treatment. Superlattices and Microstructures. 2016:90-87. DOI: 10.1016/j.spmi.2015.12.007

[41] Liu M, Qiu X, Miyauchi M, Hashimoto K. Cu(II) oxide amorphous nanoclusters grafted Ti3+ self-doped $TiO2$: An efficient visible light photocatalyst. Chemistry of Materials. 2011:23-10. DOI: 1021/cm203025b

[42] Tadic M, Kralj S, Jagodic M, Hanzel D, Makovec D. Magnetic properties of novel superparamagnetic iron oxide nanoclusters and their peculiarity under annealing treatment. Applied Surface Science. 2014:322-255. DOI: 10.1016/j. apsusc. 2014.09.181

[43] Chong Su K, Azizan SNA, Wah C, Nguyen H, Siong Chiu W, Aspanut Z, et al. Structure deformation of indium oxide from nanoparticles into nanostructured polycrystalline films by in situ thermal radiation treatment. Nanoscale Research Letters. 2013:8. DOI: 10.1186/1556-276X-8-428

[44] Flores MM, Castanedoperez R, Torresdelgado G, Marquezmarin J, Zelayaangel O. Influence of the annealing temperature on the properties of undoped indium oxide thin films obtained by the sol-gel method. Thin Solid Films, DOI. 2008:517-681. DOI: 10.1016/j.tsf.2008.07.036

[45] Sudha A, Sharma SL, Maity TK. Effects of annealing temperature on structural and electrical properties of indium oxide thin films prepared by thermal evaporation. Materials Letters. 2015:157. DOI: 10.1016/j.matlet.2015.05.050

[46] Velusamy S, Vickraman P. Annealing temperature dependent on structural, optical and electrical properties of indium oxide thin films deposited by electron beam evaporation method. Current Applied Physics. 2010;**10**:880-885. DOI: 10.1016/j.cap.2009.10.014

[47] Priya M, Arunachalam G, Ramamurthi K, Veluswamy P, Hiroya I. Effect of pH and annealing temperature on the properties of tin oxide nanoparticles prepared by sol–gel method. Journal of Materials Science: Materials in Electronics. 2017:29-658. DOI: 10.1007/s10854-017-7959-2

[48] Shahrokhi M. Tuning the band gap and optical spectra of monolayer penta-graphene under in-plane biaxial strains. Optik. 2017:205-214. DOI: 10.1016/j.ijleo.2017.02.033

[49] Endrino JL, Horwat D, Anders A, Andersson J, Gago R. Impact of annealing on the conductivity of amorphous carbon films incorporating copper and gold nanoparticles deposited by pulsed dual cathodic arc. Plasma Processes and Polymers. 2009:S438-S443. DOI: 10.1002/ppap.200931003